Evaluating a linearized Euler equations model for strong turbulence effects on sound propagation

Loïc Ehrhardt[a] and Sylvain Cheinet
Institut franco-allemand de recherches de Saint-Louis (ISL), 5 rue du Général Cassagnou, 68 300 Saint-Louis, France

Daniel Juvé and Philippe Blanc-Benon
Laboratoire de Mécanique des Fluides et d'Acoustique (LMFA), École Centrale de Lyon, 36, avenue Guy de Collongue, 69134 Écully, France

(Received 28 March 2012; revised 21 January 2013; accepted 25 January 2013)

Sound propagation outdoors is strongly affected by atmospheric turbulence. Under strongly perturbed conditions or long propagation paths, the sound fluctuations reach their asymptotic behavior, e.g., the intensity variance progressively saturates. The present study evaluates the ability of a numerical propagation model based on the finite-difference time-domain solving of the linearized Euler equations in quantitatively reproducing the wave statistics under strong and saturated intensity fluctuations. It is the continuation of a previous study where weak intensity fluctuations were considered. The numerical propagation model is presented and tested with two-dimensional harmonic sound propagation over long paths and strong atmospheric perturbations. The results are compared to quantitative theoretical or numerical predictions available on the wave statistics, including the log-amplitude variance and the probability density functions of the complex acoustic pressure. The match is excellent for the evaluated source frequencies and all sound fluctuations strengths. Hence, this model captures these many aspects of strong atmospheric turbulence effects on sound propagation. Finally, the model results for the intensity probability density function are compared with a standard fit by a generalized gamma function.
 [http://dx.doi.org/10.1121/1.4792150]

PACS number(s): 43.28.Gq, 43.28.Js, 43.28.Lv [VEO] Pages: 1922–1933

I. INTRODUCTION

The propagation of harmonic waves through media with random inhomogeneities is a subject of interest in many applications. Analytical results are available in the *weak fluctuations regime*, for which the log-amplitude variance of the wave is weak (e.g., Tatarski, 1961). However, as the wave propagates and the turbulent effects are added up, the fluctuations of the wave increase (*strong fluctuations regime*) and tend to reach an asymptotic value (*saturated fluctuations regime* or, concisely, *saturation regime*). Acoustic scenarii reaching the saturation regime are frequently met in experimental studies (see, e.g., Daigle *et al.*, 1983; Blanc-Benon and Juvé, 1993; Norris *et al.*, 2001). Some parameters, especially atmospheric ones, are difficult to measure, making the results hard to interpret (Coles *et al.*, 1995). Analytical efforts have also been carried out to understand sound propagation beyond the weak fluctuations regime (e.g., Tatarski, 1971; Jakeman, 1986; Rytov *et al.*, 1989). Significant results have been proposed, e.g., with Dashen's (1979) path integrals. However, no general analytical solution is available at present (Knepp, 1983).

In that perspective, numerical simulation is a convenient alternative for analyzing sound propagation through turbulence. Many approaches have been used to simulate the propagation of acoustic waves through random media. One may numerically solve the propagation equations for the statistical moments, e.g., the fourth order moment (e.g., Yeh *et al.*, 1975; Tur, 1982; Gozani, 1985; Spivack and Uscinski, 1988). Another approach consists of simulating sound propagation through multiple realizations of "frozen" turbulence. The sound statistics are then obtained from the sound fields realizations. Widely used propagation models for such Monte Carlo applications are the parabolic equations (PE) based models (e.g., Martin and Flatté, 1988, 1990; Gilbert *et al.*, 1990; Juvé *et al.*, 1992; Chevret *et al.*, 1996). In the absence of mean refraction, the PE may be efficiently implemented in the form of the multiple phase screen model (MPS; e.g., Knepp, 1983; Macaskill and Ewart, 1984; Spivack and Uscinski, 1989; Coles *et al.*, 1995).

Non-line-of-sight scattering effects are most important at low source frequencies (Cheinet *et al.*, 2012). The PE models are mostly adapted to near-axis propagation of harmonic waves, so they are limited to high frequency sources. Other modeling approaches are needed for lower frequency sources. There is a recent propagation model that naturally includes non-line-of-sight scattering effects, but requires higher computing time and memory resources. This is the finite-difference time-domain (FDTD) solving of the general linearized Euler equations (LEE) (Blumrich and Heimann, 2002; Salomons *et al.*, 2002; Van Renterghem, 2003; Van Renterghem and Botteldooren, 2003; Wilson and Liu, 2004; Ostashev *et al.*, 2005). Cheinet *et al.* (2012) have recently shown that this model reproduces the theoretical solutions of Tatarski (1961) for low as well as high source frequencies,

[a]Author to whom correspondence should be addressed. Electronic mail: loic.ehrhardt@isl.eu

 0001-4966/2013/133(4)/1922/12/$30.00

thereby providing a unified approach for the simulation of sound propagation through turbulence. Their analysis was focused on weak fluctuations. It thus remains to demonstrate that FDTD solving of the LEE reproduces the main features of strong turbulence effects.

The present paper addresses this issue. The objective is to propagate acoustic waves up to the saturation regime with a Monte Carlo approach using FDTD solving of the LEE as propagation model, and compare the simulated fields to available theoretical or numerical results. The quantitative evaluation of the numerical model is provided through statistical aspects. The reasons for focusing on sound wave statistics, rather than on individual instantaneous fields, are twofold; first, the sound wave statistics are well-documented, and second, they are the quantities of interest to many applications.

The paper is composed as follows. Section II presents some theoretical results on the statistics of waves propagating through turbulence. The FDTD model and the evaluation scenarii are given in Sec. III. In Sec. IV, comparisons are performed for various wave statistics: pressure mean, log-amplitude variances, transverse coherence, probability density functions (PDFs), and joint probability density (JPD). In Sec. V, the numerical propagation model is used to evaluate a standard fit of the intensity PDF by a generalized gamma distribution. Section VI summarizes the results and concludes.

II. STATISTICAL BEHAVIOR

The considered scenario is as follows: let a harmonic plane wave of frequency f, wave length λ, and wave number k propagate in the positive direction of the x-axis in a two-dimensional (2D) turbulent homogeneous medium. Turbulence is considered to have a finite outer scale. The 2D and plane wave assumptions are not necessary for the theory but make the computation time acceptable and equations simpler. Although this scenario seems restrictive, a plane wave is not rare in outdoor sound propagation scenarii because of the long propagation ranges involved. Finite outer scale turbulence is realistic for typical outdoor atmospheric turbulence. Also, the theoretical results used for comparisons have both 2D and three-dimensional (3D) formulations.

The parameters of the 2D (see above) medium are the density ρ, sound speed c, and wind velocity $\boldsymbol{u} = (u_x, u_z)$ (bold notations for vectors are used). The sound speed and density are related to the atmospheric pressure P, the temperature T, and the specific humidity q_t by (Ostashev, 1997)

$$\rho = \frac{P}{RT(1+0.61q_t)},$$
$$c = \sqrt{\gamma RT(1+0.51q_t)}, \qquad (1)$$

where the dry air characteristics are R, the gas constant, and $\gamma = C_p/C_v$, where C_p and C_v are the specific heat capacity at, respectively, constant pressure and volume. Let $\boldsymbol{r} = (x, z)$ be any point in the medium. The medium is described by the correlation functions of its parameters, the correlation function, R_τ, of any physical parameter of complex value, τ, being

$$R_\tau(\boldsymbol{r}, \boldsymbol{\delta}) = \langle \tau'(\boldsymbol{r})\tau'^*(\boldsymbol{r}+\boldsymbol{\delta})\rangle. \qquad (2)$$

Here the brackets denote ensemble averaging and the star stands for complex conjugate. The mean of the parameter is denoted τ_0 and its fluctuating value is τ', so that $\tau = \tau_0 + \tau'$. The medium is constant for $x \le 0$ and turbulent for $x > 0$. The acoustic parameters are the complex acoustic pressure $\tilde{p}$ and the time-independent part p, i.e., $\tilde{p} = pe^{2i\pi ft}$, where t is the time. This scenario is summarized in Fig. 1.

A. The $\Lambda - \Phi$ diagram

As sound propagates through turbulence, its statistical fluctuations, initially weak (weak fluctuations regime), increase (strong fluctuations regime), and tend to an asymptotic value (saturation regime). In order to give criteria for the occurrence of these regimes, Flatté (1979) introduces the $\Lambda - \Phi$ diagram for analyzing the fluctuations regimes (see also Dashen, 1979 or De Wolf, 1975).

In this diagram, two parameters are introduced. The first one is the diffraction parameter, Λ, by definition equal to $L/(6\mathcal{L}^2 k)$, where L is the propagation range and $\mathcal{L}$ is the correlation length of the turbulent atmospheric field. The definition used here for the parameter $\mathcal{L}$ is the one of Flatté (1979, p. 89); that is, $\mathcal{L}$ is obtained from the fit $\langle \mu(\mathbf{0})\mu(\Delta x, 0, 0)\rangle / \langle \mu^2(\mathbf{0})\rangle = 1 - |\Delta x/\mathcal{L}|^{q-1}$, where μ is the normalized sound speed fluctuation and q is a fit parameter, typically equal to 5/3 for atmospheric turbulence (Flatté, 1979). The second parameter is the strength parameter, Φ. By definition $\Phi^2 = \langle (k\int_0^L \mu(x)\,dx)^2\rangle \simeq k^2 L\langle \mu^2\rangle \mathcal{L}_i$. The integral length scale $\mathcal{L}_i$ and μ are given in the case of wind-only turbulence and propagation along the x-axis by $\int_{-\infty}^{+\infty} R_{u_x}(r_x, 0)\,dr_x / R_{u_x}(0,0)$ and u'_x/c_0, respectively.

According to Flatté (1979), the weak fluctuations regime occurs when $\{\Phi < 1 \text{ or } \Lambda\Phi^{\alpha/2} < 1\}$, where α is a constant related to the turbulence characteristics. A common value for the atmosphere is $\alpha = 12/5$. The saturation regime occurs when $\{\Phi > 1, \Lambda\Phi^\alpha > 1\}$. Last, the domain defined by $\{\Lambda\Phi^{\alpha/2} < 1, \Lambda\Phi^\alpha > 1\}$ is often referred as *partial saturation domain* and corresponds to the strong fluctuations regime. Thus, strong fluctuations appear as a transition

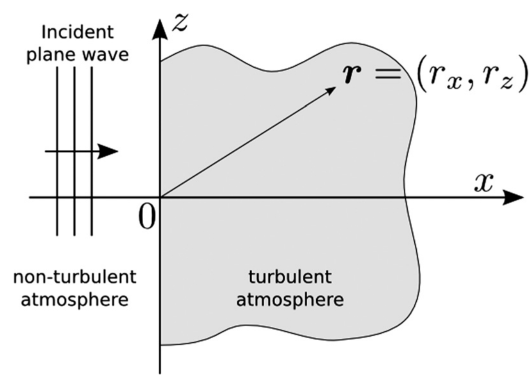

FIG. 1. Sketch of the considered acoustic scenario. A plane wave propagates in the positive direction of the x-axis (arrow direction) through atmospheric turbulence for positive x values. The turbulent volume (shaded) is considered infinite along the z-axis and positive x-axis.

between weak and saturated fluctuations regimes. These conditions lead to distinct domains in the $\Lambda-\Phi$ space. Those domains do not have sharp boundaries.

Flatté (1979, Fig. 8.6) also introduces the range-frequency diagram, equivalent to the $\Lambda-\Phi$ diagram, but more adapted to the sensitivities to the source frequency and propagation range for given turbulence statistics. An example of range-frequency diagram is given in Fig. 2. For any sound frequency, the diagram gives an estimate of the ranges at which the fluctuation regimes change.

Whatever the regime, the mean pressure decays exponentially with range, i.e.,

$$\langle p(L)\rangle = p_0 e^{-\gamma L}, \tag{3}$$

with the exponential decay factor, γ, given by an integration over the scattering angle, θ (Cheinet *et al.*, 2012)

$$\gamma = 2\pi k^3 \int_0^{\pi} \cos^2\theta \Phi_n^z\left(0, 2k\sin\frac{\theta}{2}\right) d\theta. \tag{4}$$

Here, the generalized index of fluctuations n is approximated to (Candel, 1979)

$$n = -\left(\frac{T'}{2T_0} + \frac{u'_x}{c_0}\right). \tag{5}$$

Also, $\Phi_\tau^z(x,\kappa_z)$ is the transverse spectrum of τ at plane x, i.e., the Fourier transform of $R_\tau(x,(0,\delta_z))$

$$\Phi_\tau^z(x,\kappa_z) = \int_{-\infty}^{+\infty} R_\tau(x,(0,\delta_z)) e^{-i\kappa_z\delta_z}\, d\delta_z, \tag{6}$$

and is equal to $\Phi_\tau((x,0),(0,\kappa_z))$ if Φ_τ is the spectrum of τ

$$\Phi_\tau(\boldsymbol{r},(\kappa_x,\kappa_z)) = \int_{-\infty}^{+\infty} d\delta_x \int_{-\infty}^{+\infty} R_\tau(\boldsymbol{r},(\delta_x,\delta_z)) \times e^{-i(\kappa_x\delta_x+\kappa_z\delta_z)}\, d\delta_z. \tag{7}$$

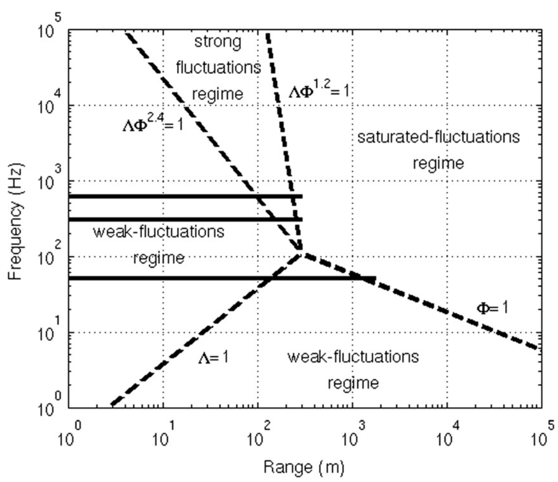

FIG. 2. Range-frequency diagram. The dashed lines and equations show the boundaries between the various fluctuations regimes. The solid lines represent the simulation sets considered in this study.

Note that a widely used expression for γ can be derived under the parabolic approximation

$$\gamma = 2\pi k^2 \int_0^{+\infty} \Phi_n^z(0,\kappa_z)\, d\kappa_z. \tag{8}$$

B. Weak fluctuations regime

At short propagation ranges, the wave fluctuations are weak (Fig. 2). The weak fluctuations regime has already been extensively studied. In particular, Tatarski (1961) has given analytical expressions for the log-amplitude variance $\sigma_\chi^2 = \langle\chi^2\rangle - \langle\chi\rangle^2$, where $\chi = \log(|p|)$, and the transverse coherence $\Gamma(L,\delta) = \langle p(L,z)p^*(L,z+\delta)\rangle$. In 2D, the equations are

$$\sigma_\chi^2(L) = 4\pi k^2 \int_0^L dx \int_0^{+\infty} \sin^2\left(\frac{\kappa_z^2(L-x)}{2k}\right)\Phi_n^z(x,\kappa_z)\, d\kappa_z, \tag{9}$$

$$\Gamma(L,\delta) = p_0 p_0^* e^{-4\pi k^2 L \int_0^{+\infty}(1-\cos(\delta\kappa_z))\Phi_n^z(0,\kappa_z)\, d\kappa_z}. \tag{10}$$

Moreover, according to Tatarski (1961) the log-amplitude and phase (of the complex pressure) are normally distributed. [Note that an error is present in Cheinet *et al.* (2012). The constant factor in the right-hand side term of their Eqs. (30) and (31) should be π instead of $\pi/2$.]

C. Strong fluctuations regime

Strong wave fluctuations occur while the partial saturation domain or the boundary $\{\Phi = 1, \Lambda > 1\}$ are crossed.

Despite many theoretical considerations (e.g., Tatarski, 1971; Jakeman, 1986; Rytov *et al.*, 1989; Dashen, 1979), the analytical expressions in this regime are limited to specific configurations such as high frequency or weak atmospheric fluctuations.

At low frequencies, a simple model derived by Brownlee (1973) can be applied. According to Brownlee (1973), when $\sqrt{\lambda L} \gg \mathcal{L}$ (i.e., when $\Lambda \gg 1$), the JPD of p at range L is the non-centered complex Gaussian distribution $\mathcal{N}_{\mathbb{C}}(p_0 e^{-\gamma L}, \sigma_{ps}^2)$, so that $\langle p\rangle = p_0 e^{-\gamma L}$; that is, the real part of p is Gaussian distributed with mean $\mathrm{Re}(p_0 e^{-\gamma L})$ and variance σ_{ps}^2 dependent on L, and the imaginary part is also Gaussian distributed with mean $\mathrm{Im}(p_0 e^{-\gamma L})$ and has the same variance, σ_{ps}^2. The value of σ_{ps}^2 can be deduced from the conservation of energy and is $|p_0^2|/2(1-e^{-2\gamma L})$. The PDF of the amplitude is then the Rice distribution, $\mathcal{R}$, also sometimes called Rice-Nakagami, given by

$$\mathcal{R}(A) = \frac{A}{\sigma_{ps}^2}\exp\left(-\frac{A^2+|\langle p\rangle|^2}{2\sigma_{ps}^2}\right) I_0\left(\frac{A|\langle p\rangle|}{\sigma_{ps}^2}\right), \tag{11}$$

where I_n is the modified Bessel function of order n. The mean and variance of A can be analytically deduced

$$\begin{cases} \langle A\rangle_B = \sigma_{ps}\sqrt{\frac{\pi}{2}}e^{-|\langle p\rangle|^2/(4\sigma_{ps}^2)}\left[\left(1+\frac{|\langle p\rangle|^2}{2\sigma_{ps}^2}\right)I_0\left(\frac{|\langle p\rangle|^2}{2\sigma_{ps}^2}\right)+\frac{|\langle p\rangle|^2}{2\sigma_{ps}^2}I_1\left(\frac{|\langle p\rangle|^2}{2\sigma_{ps}^2}\right)\right], \\ \sigma_{A\_B}^2 = \langle A^2\rangle_B - \langle A\rangle_B^2 = (|\langle p\rangle|^2 + 2\sigma_{ps}^2) - \langle A\rangle_B^2, \end{cases} \tag{12}$$

where the subscript B stands for the values under the theory of Brownlee (1973). To our knowledge, there is no direct analytical method for deriving the mean and variance of χ and intensity, I, from this PDF. Solutions can be obtained by a change of variable in the Rice distribution of A and numerical integration

$$\begin{cases} \langle \chi^n\rangle_B = \int_{-\infty}^{+\infty} \chi^n e^{\chi}\mathcal{R}(e^{\chi})\,d\chi, \\ \langle I^n\rangle_B = \int_0^{+\infty} \frac{I^n}{2\sqrt{I}}\mathcal{R}(\sqrt{I})\,dI. \end{cases} \tag{13}$$

D. Saturated fluctuations regime

The wave fluctuations increase with range and eventually saturate (Tatarski, 1971; Dashen, 1979; Jakeman, 1986; Rytov *et al.*, 1989). The complex sound pressure at the receiver in this saturation regime is the sum of many uncorrelated contributions, each of which has the same probability distribution. The complex sound pressure follows complex centered Gaussian statistics by virtue of the central limit theorem. As a result, the amplitude is Rayleigh distributed, the log-amplitude is "log-Rayleigh" as defined in Rivet *et al.* (2007), the phase is uniform in $[-\pi;\pi]$, and the intensity has an exponential distribution. The only free parameter of these PDFs is given by conservation of energy (total energy given by $|p_0^2|$). The mean and variances of the main parameters are given in Table I.

III. THE NUMERICAL SIMULATIONS

This section describes the numerical procedure used to estimate the wave statistics by a Monte Carlo approach using FDTD solving of the LEE as propagation model.

A. Atmospheric turbulence

Turbulence is described by the correlation functions of its parameters, or, equivalently, by their spectrum, Φ. To generate a turbulent atmospheric field from the given spectrum, the random fluctuations generation (RFG) algorithm described by Frehlich *et al.* (2001) and implemented in Cheinet *et al.* (2012) is used. The main idea is to sample the fluctuation spectrum, apply a random phase, and Fourier-transform to obtain the fluctuations in the physical space.

The RFG algorithm generates turbulent fields from a given spectrum. In the considered simulations there is no temperature or humidity turbulence, only wind turbulence with zero mean. The reason for this choice is discussed in Sec. III C. There are three spectra as input: Φ_{11}, Φ_{12}, and Φ_{22} denoting, respectively, the correlation of u_x, the correlation of u_z, or the cross-correlation between u_x and u_z. In order to create a statistically homogeneous, non-divergent 2D wind field, the following relation must be verified:

$$\Phi_{ij}(\boldsymbol{\kappa}) = \frac{E(\kappa)}{\pi\kappa^3}(\delta_{ij}\kappa^2 - \kappa_i\kappa_j). \tag{14}$$

As 2D turbulence is less common than the 3D turbulence, additional details on the derivation of Eq. (14) are given in Appendix A. The energy spectrum $E(\kappa)$ depends only on the norm of $\boldsymbol{\kappa}$ (isotropy). Here, the von Karman spectrum is chosen [Wilson, 1998, Eq. (96); Cheinet, 2012]

$$E^{\mathrm{vK}}(\kappa) = 2\frac{4\Gamma(17/6)}{3\sqrt{\pi}\Gamma(1/3)}\frac{\sigma^2\kappa^4L_0^5}{(1+\kappa^2L_0^2)^{17/6}}. \tag{15}$$

The decay for large κ is in $\kappa^{-5/3}$, which is consistent with the inertial convective range theory. There are predominant eddies (which size is related to L_0), and the spectrum tends to zero for small κ, removing the very large eddies (finite outer scale). Two parameters are needed for the von Karman energy spectrum: the characteristic eddy size, L_0, and the total variance of each component of the field, $\sigma^2 = \langle u_x'^2\rangle = \langle u_z'^2\rangle$. There are alternative expressions for this spectrum, e.g., with the structure parameter C_n^2.

The spectrum of Eq. (15) shows non-zero wind fluctuations at very small spatial scales. On the other hand, the sound propagation model introduced hereafter has a finite spatial resolution h (Secs. III B and III C). In the absence of specific parameterization, it is unable to account for the impact of eddies of the order of (and *a fortiori*, smaller than) the spatial resolution. In order to avoid an implicit numerical truncation, we explicitly filter all eddies smaller than $6h$ by incorporating a spectral cutoff in the energy spectrum [Eq. (15)] at wavenumbers larger than $2\pi/(6h)$. Due to the sharp decrease of the spectrum at high wavenumbers, the wind variance is only slightly reduced by this cutoff (less than 3%), and the predicted acoustic field is virtually unchanged (less than 1%) with truncations at $4h$ and $8h$.

An example of realization of wind turbulence generated from this algorithm and spectrum with $\sigma = 4\,\mathrm{m/s}$ and $L_0 = 5.0643\,\mathrm{m}$ is given in Fig. 3.

TABLE I. Mean and variances of the main acoustic parameters in the saturated fluctuations regime. γ_E is the Euler constant.

Parameter	Mean	Variance
χ	$\log(\lvert p_0\rvert/\sqrt{2}) + (\log 2 - \gamma_E)/2$	$\pi^2/24$
A	$\lvert p_0\rvert\sqrt{\pi}/2$	$\lvert p_0^2\rvert(4-\pi)/4$
$A/\langle A\rangle$	1	$(4-\pi)/\pi$
I	$\lvert p_0^2\rvert$	$\lvert p_0^4\rvert$
$I/\langle I\rangle$	1	1

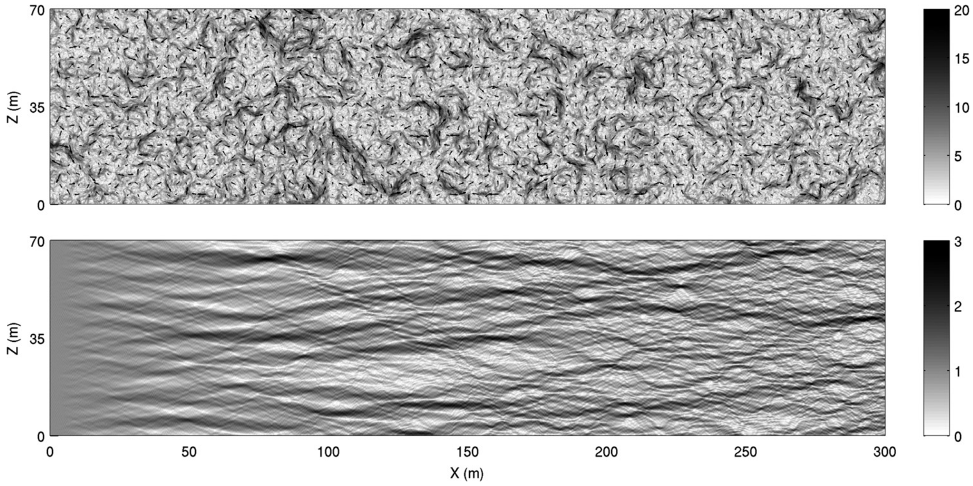

FIG. 3. (Top) Wind amplitude (color plot in m/s) and direction (arrows) generated from the RFG model, and (bottom) amplitude (normalized at 1 for $X=0$ m) of a 300 Hz plane wave propagated with the FDTD model in positive x direction through this realization of wind turbulence.

B. The FDTD model

The FDTD model used in this study has been described in Cheinet and Naz (2006), Ehrhardt and Cheinet (2010), and Cheinet *et al.* (2012). Details are given here for completeness. The prognostic equations solved by the FDTD method (i.e., the LEE) are (Blumrich and Heimann, 2002; Salomons *et al.*, 2002; Van Renterghem, 2003; Van Renterghem and Botteldooren, 2003; Wilson and Liu, 2004; Ostashev *et al.*, 2005)

$$\begin{cases} \dfrac{\partial p_a}{\partial t} = -(\boldsymbol{u}\cdot\nabla)p_a - \rho c^2\nabla\cdot\boldsymbol{w_a} + \rho c^2 Q, \\ \dfrac{\partial \boldsymbol{w_a}}{\partial t} = -(\boldsymbol{u}\cdot\nabla)\boldsymbol{w_a} - (\boldsymbol{w_a}\cdot\nabla)\boldsymbol{u} - \dfrac{\nabla p_a}{\rho} + \dfrac{\boldsymbol{F}}{\rho}. \end{cases} \quad (16)$$

Here, p_a and $\boldsymbol{w_a}$ are the acoustic pressure and particle velocity, respectively, of real value $[p_a = \mathrm{Re}(\tilde{p})]$, and the parameters Q and $\boldsymbol{F}$ are the mass and force sources, respectively. The simulated acoustic fields are obtained by the integrating of Eq. (16) over time. The fields are stored on an equidistant half-staggered mesh. The spatial derivatives are approximated by the means of 4th order central finite differences. A 4th order Runge-Kutta time integration is used. Typically for such numerical integration methods the time step, dt, is required to be less than Ch/c, where $C \simeq 0.74 < 1$ is the Courant number, and the spatial step h is required to be less than 1/16 of the acoustic source wavelength. Absorbing boundary conditions, used to simulate free field propagation, are modeled by specific porous media where there is no jump of impedance at the interface, and the sound resistivity is constantly increasing (see Wilson and Liu, 2004). Compared to the model detailed in Cheinet *et al.* (2012), the numerical code has been adapted for massive parallel processing on a computational cluster with the MPI and OpenMP standards. These are the only differences with the model used in Cheinet *et al.* (2012). The motivations for these changes are that a 4th order scheme requires a lower λ/h ratio for identical accuracy, allowing a decrease in the number of nodes for identical physical domain and hence faster computation. This, with the parallel implementation of the FDTD model on a cluster, made the FDTD simulation of sound propagation in the saturation regime feasible. After the FDTD computation, phase and amplitude (that is, complex pressure) of the propagated wave are obtained by Fourier-transforming on the source frequency the time-dependent FDTD results, p_a,

$$p(\boldsymbol{r}) = \frac{2}{N}\sum_{\eta=1}^{N} p_a(\boldsymbol{r}, t_0 + \eta\ dt)e^{2i\pi f\eta dt}, \quad (17)$$

where t_0 is a time at which sound amplitude is quasi-stationary and Ndt is a time duration that must be greater than a period of the source, i.e., $Ndt > 1/f$. Hereafter, $N = 100$ is chosen.

An example of propagation with the FDTD model of 300 Hz plane wave through the above realization of wind turbulence is given in Fig. 3. The amplitude of the propagated wave features some typical sound paths in the direction of propagation (Blanc-Benon *et al.*, 1992; Hugon-Jeannin, 1992).

C. Scenarii and numerical details

The choice of the acoustic propagation scenario is limited by the strong computational needs of FDTD simulations in general. The chosen scenario allows the simulation of strong and saturated sound fluctuations by a Monte Carlo approach using a FDTD solving of the LEE for audible or near-audible frequencies and for realistic atmosphere. The scenario is described below with numerical details.

Typical temperature fluctuations in the atmosphere hardly reach a few degrees, leading to $\langle\mu^2\rangle$ of the order of 10^{-5} whereas wind fluctuations can reach some m/s, leading to $\langle\mu^2\rangle$ of the order of 10^{-4}. Sound is thus more influenced by wind fluctuations than by temperature fluctuations (Ostashev and Wilson, 2000; Cheinet, 2012). Wind fluctuations are therefore considered here in order to reach the saturation regime. Here we use $\sqrt{\langle|u'_x|^2\rangle} = \sqrt{\langle|u'_z|^2\rangle} = 4\,\mathrm{m/s}$ and $L_0 = 5.0643$ m. The corresponding range-frequency diagram is plotted in Fig. 2.

A harmonic plane wave is propagating through such turbulence. Three sets of simulations are computed for source

TABLE II. Numerical details for each set of simulations.

	Scenario		
Source frequency	50 Hz	300 Hz	600 Hz
Propagation range	1800 m	300 m	300 m
	Turbulence		
σ	4 m/s	4 m/s	4 m/s
L_0	5.0643 m	5.0643 m	5.0643 m
	RFG		
Generated turbulence domain	4800 $\times$ 1000 nodes	4800 $\times$ 1000 nodes	9600 $\times$ 2000 nodes
	2016 $\times$ 420 m^2	336 $\times$ 70 m^2	336 $\times$ 70 m^2
Grid step	42 cm	7 cm	3.5 cm
Turbulence Tukey smoothing width	100 nodes	100 nodes	200 nodes
	42 m	7 m	7 m
Small eddies cutoff	6 nodes	6 nodes	6 nodes
	2.52 m	0.42 m	0.21 m
	FDTD		
Total computational domain	5000 $\times$ 1000 nodes	5000 $\times$ 1000 nodes	10000 $\times$ 2000 nodes
	2100 $\times$ 420 m^2	350 $\times$ 70 m^2	350 $\times$ 70 m^2
Grid step	42 cm	7 cm	3.5 cm
Nodes bounded to turbulent fields	201–5000 $\times$ 1–1000	201–5000 $\times$ 1–1000	401–10000 $\times$ 1–2000
Left and right absorbing layers width	200 nodes	200 nodes	400 nodes
	84 m	14 m	14 m
Time step	0.9 ms	0.15 ms	0.075 ms
Total simulation duration	10.8 s	1.8 s	1.8 s
	12 000 time iterations	12 000 time iterations	24 000 time iterations
	Results		
Nodes extracted for postprocessing	201–4600 $\times$ 1–1000	201–4600 $\times$ 1–1000	401–9200 $\times$ 1–2000

frequencies 50 Hz, 300 Hz, and 600 Hz and propagation lengths of, respectively, 1800 m, 300 m, and 300 m. As can be seen in the range-frequency plot, all fluctuations regimes are covered with these sets of simulations.

We now give the numerical details for the 50 Hz set. Table II summarizes these aspects for all the sets. The computational domain used in the FDTD model is 2100×420 m^2 wide and the grid spacing is 42 cm; thus there are 5000 $\times$ 1000 nodes. Turbulent wind fluctuations are bound to nodes 201–5000 $\times$ 1–1000. There is no wind at the other nodes. Absorbing layers are implemented on the left and right sides of the domain. They are 200 nodes (84 m) thick. The harmonic acoustic plane wave is set at the right side of the left absorbing layer and, to assume perfect planarity, the domain is periodic on the top and bottom boundaries, which is in concordance with the RFG-generated turbulent fields. The wave is thus generated at $x = 0$ (right side of left absorbing boundary condition), propagates through turbulence (longest path of the propagation), and is finally absorbed by the right boundary condition. The turbulent field generated is 2016 $\times$ 420 m^2 wide and the grid spacing is the same as above, i.e., 4800 $\times$ 1000 nodes are used. The transverse size of the domain is much greater than L_0, allowing a satisfactory description of the larger eddies. In the first 100 nodes after the source, the wind fluctuations are reduced by a Tukey window such that the turbulence begins gradually. The results are taken over the nodes 201–4600 $\times$ 1–1000 (propagation length of 1848 m). The time step is 0.9 ms and 12 000 time iterations were performed.

The number of nodes required for efficient absorption could be reduced by using the efficient and popular perfectly matched layers (PML) absorbing conditions (Bérenger, 1994, 1996). Still, only a weak proportion of nodes are used for absorption (8%) so no significant change in the computational time is expected by the implementation of PMLs.

Last, a large number of simulations per set are required if one wishes to obtain reasonable convergence of the statistical moments and PDFs. There were 1024 simulations computed for the 50 Hz and 300 Hz sets. Only 200 simulations were computed for the 600 Hz set due to the higher computational cost, which appears to be sufficient; see Sec. IV.

For each frequency set, a single simulation without turbulence was also conducted in order to get p_0 from the FDTD model, and also to check the numerical accuracy of the model (efficient absorption, no issues arising from the choice of boundaries, numerical steps, etc.).

IV. RESULTS

The following statistics of the wave are now presented and compared to available theoretical or numerical results: amplitude of the mean pressure $|\langle p \rangle|$, log-amplitude variance $\sigma_\chi^2 = \langle \chi^2 \rangle - \langle \chi \rangle^2$, transverse correlation of the pressure, JPD of the complex pressure, and PDFs of phase and amplitude. Because of the Tukey smoothing in the computations, for all theories considered, the origin of turbulence is taken as the middle of the Tukey window (in the 50 Hz set for example, 21 m after the sound origin).

A. First and second moments

The mean pressure decays exponentially [see Eq. (3)] over the full propagation range (Cheinet *et al.*, 2012). The FDTD model is consistent with these results, as can be seen in Fig. 4. In the 300 Hz and 600 Hz sets, the γ factor can be taken under the parabolic approximation [Eq. (8)]. The results compare well and in this sense, the FDTD model reproduces well the theoretical exponential decay. For the 50 Hz set, turbulence locally scatters sound not only in the line-of-sight (Cheinet *et al.*, 2012); hence, the parabolic approximation is not valid. The γ factor, which is used for evaluating the exponential decay, is calculated from Eq. (4). The match with theory is excellent. At the longest considered propagation range, the mean pressure amplitude has lost about 40% of its initial value for the 50 Hz set. The saturation regime is not fully reached yet. The loss is 96% for the 300 Hz set and nearly 100% for the 600 Hz set, which suggests that the constant part of the wave is removed, making it fully random at those ranges.

Figure 5 shows the variance of log-amplitude with range. The statistics obtained with the FDTD models are compared to some analytically derived counterparts. The first one is from Tatarski's (1961) theory in the weak fluctuations regime. As expected, the FDTD model follows exactly Tatarski (1961) as long as σ_χ^2 remains weak. As expected from above, the FDTD result does not reach saturation in the 50 Hz set. The value of σ_χ^2 at which the FDTD-simulated log-amplitude variance saturates in the other sets fully agrees with the theoretical value of $\pi^2/24$ (see Table I). It has also been checked that both $\sigma_A^2 = (\langle A^2 \rangle - \langle A \rangle^2)/\langle A \rangle^2$ and $\sigma_I^2 = (\langle I^2 \rangle - \langle I \rangle^2)/\langle I \rangle^2$ tend to their theoretical limiting values of $(4-\pi)/\pi$ and 1, respectively.

In order to evaluate the FDTD results beyond the weak or saturated fluctuations regimes, MPS simulations have been realized for the same configurations. The MPS technique used in this study is detailed in Appendix B. The phase screens considered are directly the RFG-generated turbulent fields used in the FDTD computations. There are thus 4800 phase screens for each realization. As for the FDTD model, the statistics are obtained from multiple realizations. The log-amplitude variance given from the MPS model is plotted for the three frequency sets (Fig. 5). The match between the two numerical models is excellent over the full propagation range for the 300 Hz and 600 Hz sets. The strong fluctuations regime is thus well reproduced by FDTD solving of the LEE in these sets. In the 50 Hz set, the match is good but a slight difference is visible between the FDTD and MPS results. As discussed above, the parabolic approximation is not valid for low frequencies, so the MPS model is not applicable. The theory of Brownlee (1973) is limited to configurations where $\Lambda \gg 1$. For the 300 Hz and 600 Hz sets, Λ is always smaller than 0.4 (since for the considered turbulence, $\mathcal{L} = 5$ m) so this theory is not applicable. In the 50 Hz set, however, $\Lambda > 2$ above 300 m. The theory is then applicable and is plotted for this simulation set using the general expression for γ, Eq. (4). The FDTD result matches this model. This validates both the FDTD modeling of the LEE and Brownlee's (1973) theory in the strong fluctuations regime when $\Lambda \gg 1$, i.e., at low frequencies. In summary, the log-amplitude variance is reliably

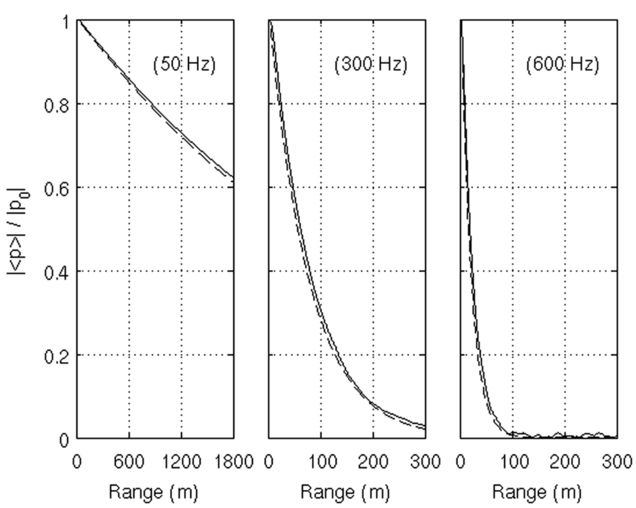

FIG. 4. Normalized amplitude of the mean pressure as function of range for a harmonic source of 50 Hz (left), 300 Hz (middle), and 600 Hz (right). The solid line represents the results obtained from the FDTD model and the dashed line represents the theoretical exponential decay. In the 50 Hz set, γ is calculated from Eq. (4), whereas in the 300 Hz and 600 Hz sets, it is calculated from Eq. (8).

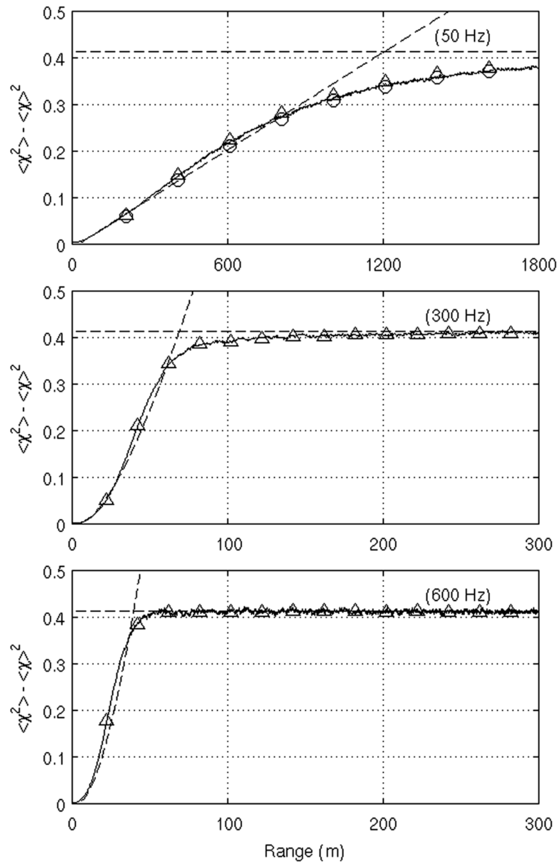

FIG. 5. Log-amplitude variance with range for a harmonic source of 50 Hz (top), 300 Hz (middle), and 600 Hz (bottom). The solid line represents the results obtained from the FDTD model. The dashed lines are the limiting values for the saturation regime (horizontal line) and Tatarski's (1961) expression in the weak fluctuations regime. Triangles are the MPS simulation results, circles in the 50 Hz set are Brownlee's (1973) theoretical results.

reproduced by a Monte Carlo approach using FDTD solving of the LEE as propagation model over all the considered frequencies and fluctuations regimes.

Figure 6 shows Γ for the 600 Hz set at various propagation ranges. Like $|\langle p \rangle|$, the FDTD and analytical expression [Eq. (10)] match at all ranges. The match is similar for the 300 Hz set, but in the 50 Hz set, the theory is no longer comparable to simulations. As discussed above, this can be explained by the inapplicability of the parabolic approximation at low frequencies.

B. Joint probability density and probability density function

A useful analytical and visual parameter for illustrating the effects of turbulence on sound propagation is the JPD of p, that is, the probability for p to have a certain complex value. The integration over all arguments (angles) gives the log-amplitude/amplitude/intensity PDF. When integrated over the module, it gives the phase PDF. Also, it shows the possible correlation between log-amplitude and phase, or between $\mathrm{Re}(p)$ and $\mathrm{Im}(p)$, through its general shape. The JPDs calculated from the sets of simulations are given in Fig. 7.

In the 50 Hz set, the JPDs are as described in Brownlee's (1973) theory, that is, non-centered Gaussian distribution. This provides an additional qualitative validation of both this theory and the FDTD model in this low frequency case. The JPD at maximum propagation range is not centered, since the saturation regime is not fully reached (Fig. 4). At 300 Hz, the fluctuations mainly occur on phase in the first propagation ranges, which is consistent with theory (Tatarski, 1961; Flatté, 1979) and leads to a croissant-shaped JPD. When the saturated regime is reached, the shape is circular and centered matching the complex centered Gaussian statistics. An eye-catching effect here is the non-symmetry toward the real axis, meaning significant correlation between χ and ϕ. Because of the chosen conventions, a counterclockwise shift stands for phase lateness, which means that the wave slows down, resulting in refocusing and higher amplitude. This explains the general trend of larger amplitudes at negative arguments (angles). The opposite deduction can be made for clockwise shift. This non-negligible dependence is described by the cross-correlation given by Tatarski (1961). At 600 Hz, the general shapes of the JPDs are similar to the 300 Hz, with more pronounced evolution with range, as expected.

The PDFs of the normalized statistics, $\phi - \arg(p_0)$ and $A/\langle A \rangle$, obtained in the 300 Hz set are given in Fig. 8 along the propagation range. The initial PDFs spread as the wave propagates from normal to uniform for ϕ, and from log-normal to Rayleigh for A. The simulated PDFs compare well with the theoretical asymptotic PDFs. It has also been checked that the other PDFs follow theory—normal to log-Rayleigh for χ and log-normal to exponential for I. The comparison results are the same for the 600 Hz set. There is no available theoretical distribution in the transitional regime for these sets. However for the 50 Hz set, Brownlee's (1973) theory provides the JPD at ranges larger than 300 m, where $\Lambda > 2$, and thus also the PDFs. In Fig. 9, the FDTD-predicted PDFs of $A/\langle A \rangle$ are compared to the theoretical Rician distributions. The match is excellent when $\Lambda > 4$.

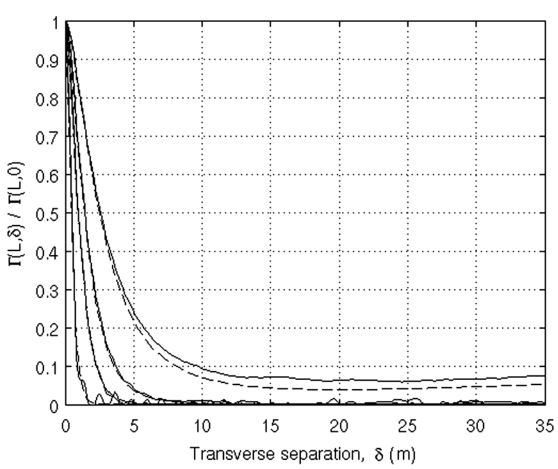

FIG. 6. Transverse coherence as a function of transverse separation for different propagation ranges for a harmonic source of 600 Hz. The solid lines represent the results obtained from the FDTD model and the dashed lines give Tatarski's (1961) theoretical expression in the weak fluctuations regime. The propagation ranges are, from top to bottom, 30 m, 60 m, 100 m, and 300 m.

V. DISCUSSION

In Sec. IV, the FDTD model has been shown to accurately reproduce the turbulence-induced statistical effects on wave propagation. In this section, it is used as a tool to evaluate a common fit for the intensity PDF.

This fit was first proposed in the late 1980s (Ewart and Percival, 1986; Ewart, 1989). The conjecture is that the intensity probability distributions are described by the generalized gamma ($G\Gamma$) distribution first introduced by Stacy (1962). This seems to be consistent with the first simulations of the authors of the conjecture and also with experimentation (Blanc-Benon and Juvé, 1993). The $G\Gamma$ distribution generally needs three parameters, but one is imposed by the assumption that $\langle I \rangle$ is constant (and taken equal to 1 here). The distribution is thus the following:

$$G\Gamma_{k,b}(I) = \frac{b\mu^k}{\Gamma(k)} I^{bk-1} e^{-\mu I^b}. \tag{18}$$

Here $\mu = [\Gamma(k+1/b)/\Gamma(k)]^b$ and the two parameters are k and b. This distribution provides a smooth transition from the log-normal distribution (in the weak fluctuations regime, when $k \to \infty$) to the exponential distribution (in the saturation regime, when $k = b = 1$). Prescribing the evolution of the parameters as the sound propagates remains an open problem.

The $G\Gamma$ distribution is not the only distribution proposed for the PDF of the intensity. Among the plethora of models proposed in the literature there are, for instance, the K-distribution (Jakeman and Pusey, 1976), the I-K distribution, the Furutsu distribution (Flatté *et al.*, 1994), or

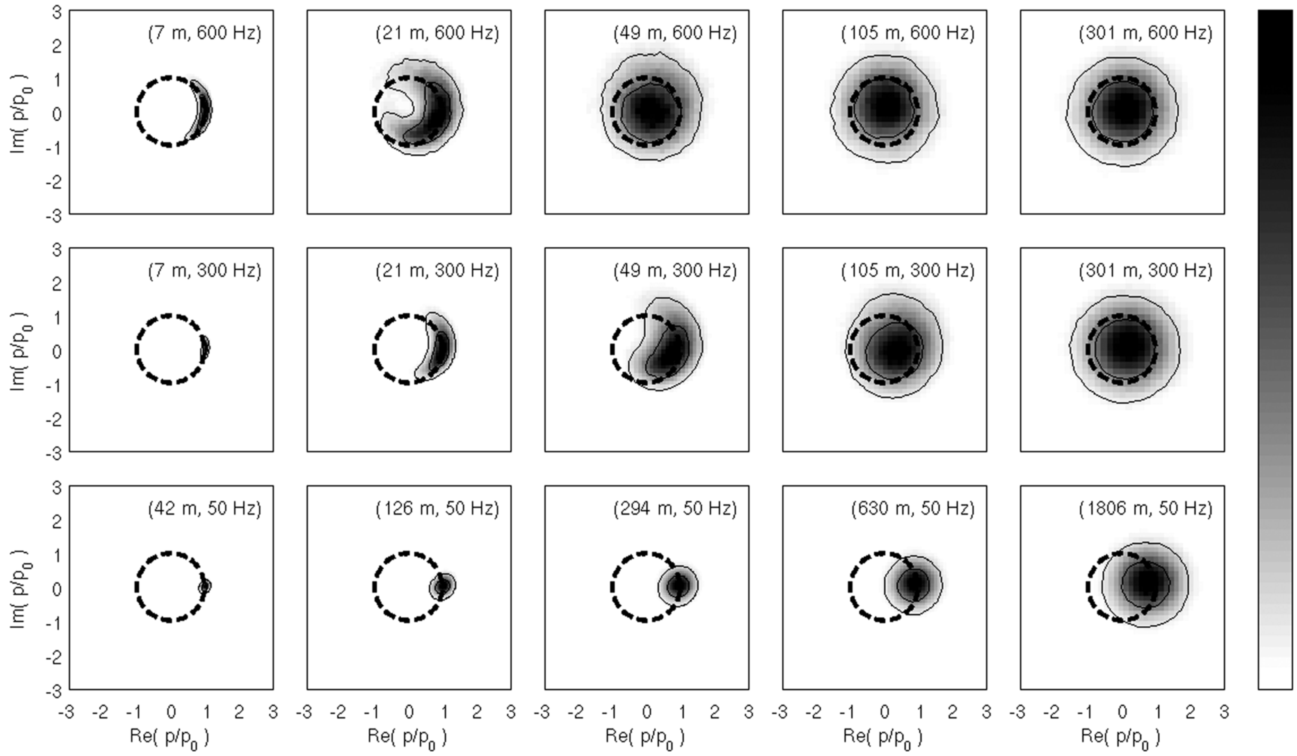

FIG. 7. Joint probability density of the complex pressure for various propagation ranges and sets (given in brackets in top-right corner on each plot) obtained from the FDTD model. Colormap is linear between zero (in white) and the maximum value (in black). The dashed circle is the unit circle and the solid lines are contours of iso-probability: 90% of the sample lie within the outer border and 50% within the inner border.

Beckman distribution (Hill and Frehlich, 1997). Some authors propose convolutions between different distributions, such as the modulated *K*- and *I*-*K* distributions (Flatté *et al.*, 1994), or log-normally modulated exponential and Rician distributions (Churnside and Hill, 1987; Churnside and Frehlich, 1989). Most of these distributions can reproduce the known asymptotical distributions in the weak fluctuations regime (log-normal) and saturation regime (exponential). In this study only the $G\Gamma$ distribution is evaluated because of its simple analytical expression (McLaren *et al.*, 2012) and as the objective is to show the potential of the FDTD model in addressing this problem.

Assuming that the intensity PDF is described by the $G\Gamma$ distribution, it is possible to determine the evolution of the (k, b) parameters with range from the FDTD simulations. The 300 Hz set is chosen for this analysis. The simplest

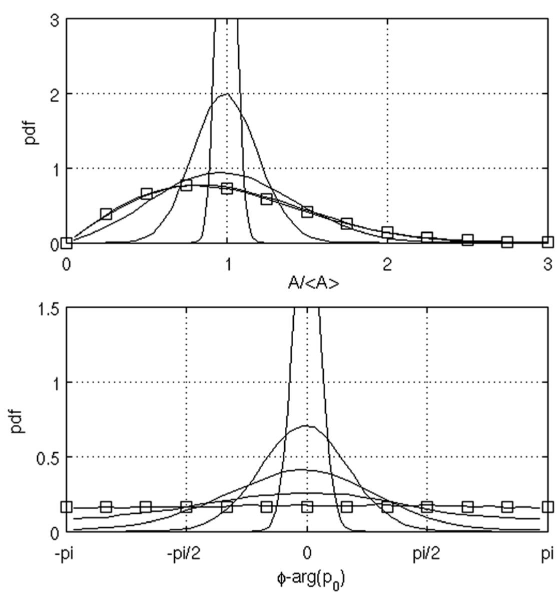

FIG. 8. Probability density functions of the normalized amplitude (top) and phase (bottom) for the 300 Hz set at different propagation ranges (7 m, 21 m, 49 m, 105 m, and 301 m) obtained from the FDTD model. The PDFs for the shorter propagation range overflow the figure. The theoretical PDF in the saturation regime is shown with squares.

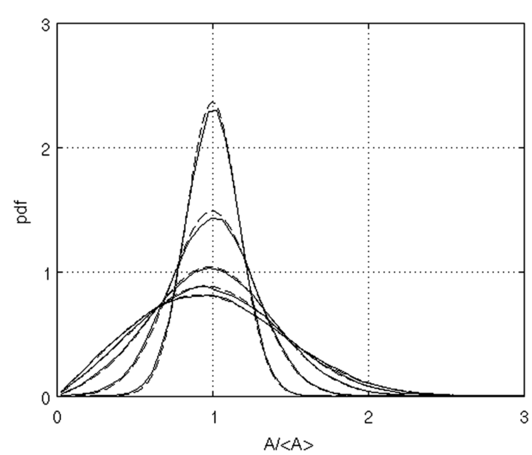

FIG. 9. Probability density functions of the normalized amplitude for the 50 Hz set at five propagation ranges (126 m, 294 m, 360 m, 966 m, and 1302 m). The solid lines are from the FDTD model and the dashed lines from Brownlee's (1973) theory. At these propagation ranges, Λ is, respectively, 0.92, 2.15, 4.60, 7.05, and 9.50.

method, consisting of solving the conjugated non-linear equations

$$\begin{cases} \dfrac{\langle I^2\rangle}{\langle I\rangle^2} = \dfrac{\Gamma(k)\Gamma(k+2/b)}{\Gamma^2(k+1/b)}, \\ \dfrac{\langle I^3\rangle}{\langle I\rangle^3} = \dfrac{\Gamma^2(k)\Gamma(k+3/b)}{\Gamma^3(k+1/b)}, \end{cases} \tag{19}$$

where $\langle I\rangle$, $\langle I^2\rangle$, and $\langle I^3\rangle$ are computed from the FDTD-simulated samples, does not provide accurate results as two different distributions may have very close first three moments (Ewart and Percival, 1986; Ewart, 1989). The method used here is a determination of the couple of parameters $(1/k,\ b)$ minimizing the *Cramer von Mises criterion*—least squares on the cumulative density function at each propagation range. The obtained parameters are shown with range on Fig. 10. At small ranges, k is infinite (log-normal distribution) and at long ranges k and b both tend to 1 (exponential distribution). It has been qualitatively checked that the obtained generalized gamma distribution fits the simulated one. All the previously presented amplitude-related statistics can be deduced from this fit.

After the range 80 m, the fit gives $kb = 1$. This suggests that a one-parameter law is sufficient for strong enough wave fluctuations, which is consistent with studies showing good agreement between a one-parameter PDF and experimental data (Churnside and Hill, 1987).

VI. CONCLUSION

Sound is influenced by atmospheric turbulence. Even in an *a priori* simple configuration, that is, 2D harmonic plane wave propagation through homogeneous wind-only turbulence, the wave behavior is complex and not fully understood. Yet, such scenarii are of practical interest, therefore many analytical, experimental, and numerical efforts have been made to increase knowledge in this field. One major issue is the lack of solutions, be they analytical, experimental, or numerical, valid for all realistic scenarii. Most often there are limitations on the source frequency (as in Brownlee, 1973), the intensity of sound fluctuations (as in Tatarski, 1961) or the geometry of the configuration (as in parabolic equations simulations). Also, most of the quantitative results are only available for some particular statistical parameters of the wave.

FDTD solving of the LEE is a more computationally intensive model which overcomes these limitations. It has already been shown to capture the physics of sound propagation through turbulence at high and low frequencies for weak sound fluctuations (Cheinet *et al.*, 2012). The present study is intended to assess stronger wave fluctuations. The case of 2D harmonic plane wave propagation through homogeneous wind turbulence is considered. FDTD simulations are performed for multiple realizations of turbulence and the obtained wave statistics are compared to various theoretical or numerical results. For low acoustic source frequencies, the model of Brownlee (1973) is used. For higher frequencies, MPS simulations are used for evaluation. Also, for weak fluctuations regime, Tatarski's (1961) theory is used and for the saturation regime, Gaussian statistics are considered (see, e.g., Dashen, 1979 or Flatté, 1979).

The amplitude of the mean complex pressure, the log-amplitude variance, and the transverse coherence are consistent between the FDTD model and the compared theoretical or numerical results. The joint probability density (JPD) function of the complex pressure also gives valuable results. In the low frequency case, the FDTD result matches the theoretical expectation (non-centered complex Gaussian distribution). For higher frequencies, the behavior is also consistent—the phase fluctuations are greater than log-amplitude fluctuations and there is notable cross-correlation between these two parameters. In the saturation regime, the JPD is a centered Gaussian as predicted by theory. Last, the probability density functions (PDF) of the phase and amplitude match theoretical PDFs in the saturation regime. For low frequencies, the available theoretical PDFs are in agreement with the FDTD model. These overall comparisons lead to the conclusion that a Monte Carlo approach using a FDTD solving of the LEE as propagation model reproduces the known statistical behavior for harmonic plane wave propagation through turbulence for all fluctuation regimes. Finally, the FDTD model is used as a tool to evaluate the fitting of the intensity PDF by a generalized gamma function. The FDTD simulations give the evolution of the parameters of this distribution with range for one of the simulated source frequencies.

In the future, it could be valuable to further investigate the instantaneous pressure fields (Fig. 3) which contain additional physics from statistical quantities.

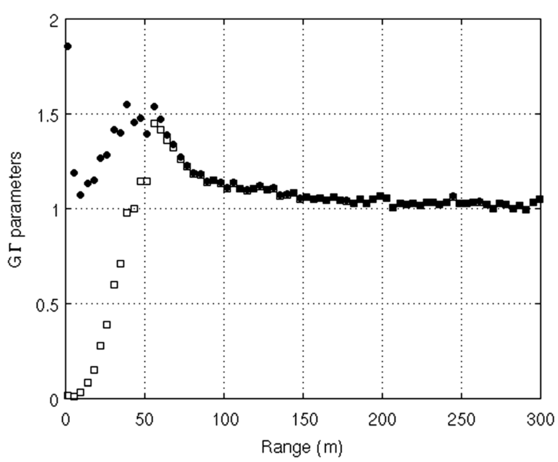

FIG. 10. The two parameters of the $G\Gamma$ distribution fitting the simulated PDF of the intensity for the 300 Hz set. The white squares give $1/k$ and the black circles give b.

ACKNOWLEDGMENTS

The ISL Aerodynamics Department is acknowledged for providing access to their computational cluster. The authors thank the anonymous reviewers for their pertinent remarks and suggestions, which helped improve the paper.

APPENDIX A: TWO-DIMENSIONAL SPECTRA OF WIND TURBULENCE

The aim of this appendix is to provide more details concerning the derivation of Eq. (14). The 3D case as described in Batchelor (1953) is first recalled and the differences with the 2D equivalent are given.

According to Batchelor (1953, Eqs. 3.4.10, 3.3.5, and 2.4.7), the 3D spatial spectra Φ_{ij} of a non-divergent vector field are given by

$$\Phi_{ij}(\boldsymbol{k}) = A(k)(k_i k_j - \delta_{ij} k^2), \tag{A1}$$

where $\boldsymbol{k}$ is a 3D vector field, k_i denotes its ith component and k its norm, δ_{ij} is the Kronecker symbol, and $A(k)$ any function. The energy spectrum E can be obtained from Φ_{ij} (Batchelor 1953, Eqs. 3.1.5 and 3.1.2)

$$E(k) = \frac{1}{2}\int\int(\Phi_{11} + \Phi_{22} + \Phi_{33})(\boldsymbol{k})\, dS(k), \tag{A2}$$

where the integration is calculated on the surface of a sphere of radius k. Equation (A2) simplifies to

$$E(k) = \frac{1}{2}(-2k^2 A(k))(4\pi k^2) = -4\pi k^4 A(k). \tag{A3}$$

The spatial spectra can therefore be written as function of energy spectrum only, leading to the well-known [see, e.g., Wilson, 1998, Eq. (16)] relation

$$\Phi_{ij}(\boldsymbol{k}) = \frac{E(k)}{4\pi k^4}(\delta_{ij} k^2 - k_i k_j). \tag{A4}$$

The 2D case presents only one difference. Equation (A1) remains valid, but the integration on Eq. (A2) is calculated on the perimeter of a circle of radius k. Thus

$$\begin{aligned} E(k) &= \frac{1}{2}\int(\Phi_{11} + \Phi_{22})(\boldsymbol{k})\, dl(k) \\ &= \frac{1}{2}(-k^2 A(k))(2\pi k) = -\pi k^3 A(k). \end{aligned} \tag{A5}$$

And finally

$$\Phi_{ij}(\boldsymbol{k}) = \frac{E(k)}{\pi k^3}(\delta_{ij} k^2 - k_i k_j)\ . \tag{A6}$$

APPENDIX B: THE MULTIPLE PHASE SCREEN NUMERICAL MODEL

In this appendix, the MPS numerical model is described. This model is an efficient implementation of the PE model in case of absence of mean refraction, and therefore also comes with a high-frequency limitation. MPS simulations have been widely used for studying sound propagation through random media (Knepp, 1983; Macaskill and Ewart, 1984; Spivack and Uscinski, 1989; Coles *et al.*, 1995). The acoustic fields given by MPS simulations have been compared to other theories, other models, and experimental data in many cases with good agreement. It is therefore a well-established model.

This model allows the calculation of sound pressure by step-by-step iteration over the propagation range. The propagation through turbulence is separated into two independent physical processes. First, the turbulent atmosphere is modeled by multiple screens separated by a given distance dx. As the atmospheric fluctuations are assumed to be small, the effect of those screens on sound crossing them is a simple phase change—leading to the names of *phase* screens. If one considers a phase screen located at x, the complex sound pressure just after the screen $p(x^+)$ is related to the complex sound pressure just before the screen $p(x^-)$ by

$$p(x^+, z) = p(x^-, z)e^{-ikn(x,z)dx}, \tag{B1}$$

where n is the generalized index of fluctuations given in Eq. (5). The second physical process is the propagation between two adjacent phase screens. Free field propagation is considered (no turbulence). The complex sound pressure just before the next phase screen $p(x + dx)$ is obtained by application of the free-field propagation factor $\exp(iK^2 dx/(2k))$ in the transverse spectral space and of a factor $\exp(-ikdx)$ in the physical space (Knepp, 1983; Coles *et al.*, 1995)

$$\begin{aligned} p(x+dx, z) = {} & \mathcal{F}^{-1}\left[\exp\left(\frac{iK^2 dx}{2k}\right)\mathcal{F}[p(x^+, z)](K)\right](z) \\ & \times e^{-ikdx}, \end{aligned} \tag{B2}$$

where $\mathcal{F}[p(x,z)](K)$ is the spatial transverse Fourier transform of $p(x,z)$ and $\mathcal{F}^{-1}[p(x,K)](z)$ is the inverse spatial transverse Fourier transform of $p(x,K)$. This second physical process causes the sound amplitude fluctuations arising from phase fluctuations. The MPS method thus consists in successively applying Eq. (B1) for a phase screen and Eq. (B2) to reach the next phase screen. It is unconditionally stable, consistent, and convergent (Jenu and Bebbington, 1994).

Batchelor, G. K. (**1953**). *Homogeneous Turbulence* (Cambridge University Press, New York), Chaps. 2 and 3.

Bérenger, J. P. (**1994**). "A perfectly matched layer for the absorption of electromagnetic waves," J. Comput. Phys. **114**, 185–200.

Bérenger, J. P. (**1996**). "Three-dimensional perfectly matched layer for the absorption of electromagnetic waves," J. Comput. Phys. **127**, 363–379.

Blanc-Benon, P., and Juvé, D. (**1993**). "Intensity fluctuations of spherical acoustic waves propagating through thermal turbulence," Waves Random Media **3**, 71–83.

Blanc-Benon, P., Juvé, D., and Hugon-Jeannin, Y. (**1992**). "Propagation of acoustic waves through thermal turbulence: A numerical study of intensity fluctuations," in *European Conference on Underwater Acoustics*, edited by M. Weydert (Elsevier Applied Science, London), pp. 284–287.

Blumrich, R., and Heimann, D. (**2002**). "A linearized Eulerian sound propagation model for studies of complex meteorological effects," J. Acoust. Soc. Am. **112**, 446–455.

Brownlee, L. R. (**1973**). "Rytov's method and large fluctuations," J. Acoust. Soc. Am. **53**, 156–161.

Candel, S. (**1979**). "Numerical solution of wave scattering problems in the parabolic approximation," J. Fluid Mech. **90**, 465–507.

Cheinet, S. (**2012**). "A numerical approach to sound levels in near-surface refractive shadows," J. Acoust. Soc. Am. **131**, 1946–1958.

Cheinet, S., Ehrhardt, L., Juvé, D., and Blanc-Benon, P. (**2012**). "Unified modeling of turbulence effects on sound propagation," J. Acoust. Soc. Am. **132**, 2198–2209.

Cheinet, S., and Naz, P. (**2006**). “On-going ISL research in modelling acoustic propagation in the atmosphere,” NATO SET-107/RSY20/MSE Symposium, Amsterdam, The Netherlands.

Chevret, P., Blanc-Benon, P., and Juvé, D. (**1996**). “A numerical model for sound propagation through a turbulent atmosphere near the ground,” J. Acoust. Soc. Am. **100**, 3587–3599.

Churnside, J. H., and Frehlich, R. G. (**1989**). “Experimental evaluation of log-normally modulated Rician and IK models of optical scintillation in the atmosphere,” J. Opt. Soc. Am. A **6**, 1760–1766.

Churnside, J. H., and Hill, J. R. (**1987**). “Probability density of irradiance scintillations for strong path-integrated refractive turbulence,” J. Opt. Soc. Am. A **4**, 727–733.

Coles, W. A., Filice, J. P., Frehlich, R. G., and Yadlowsky, M. (**1995**). “Simulation of wave propagation in three-dimensional random media,” Appl. Opt. **34**, 2089–2101.

Daigle, G., Piercy, J., and Embleton, T. (**1983**). “Line-of-sight propagation through atmospheric turbulence near the ground,” J. Acoust. Soc. Am. **74**, 1505–1513.

Dashen, R. (**1979**). “Path integrals for wave in random media,” J. Math. Phys. **20**, 894–920.

De Wolf, D. A. (**1975**). “Propagation regimes for turbulent atmospheres,” Radio Sci. **10**, 53–57, doi:10.1029/RS010i001p00053.

Ehrhardt, L., and Cheinet, S. (**2010**). “Développement et évaluation d’un code de propagation acoustique en domaine temporel (Development and evaluation of an acoustic propagation code),” 10e Congrès Français d’Acoustique, Lyon, France. Available at http://cfa.sfa.asso.fr/cd1/data/articles/000560.pdf (Last viewed March 26, 2012).

Ewart, T. E. (**1989**). “A model of the intensity probability distribution for wave propagation in random media,” J. Acoust. Soc. Am. **86**, 1490–1498.

Ewart, T. E., and Percival, D. B. (**1986**). “Forward scattered waves in random media—The probability distribution of intensity,” J. Acoust. Soc. Am. **80**, 1745–1753.

Flatté, S. M. (**1979**). *Sound Transmission Through a Fluctuating Ocean* (Cambridge University Press, New York), Chaps. 6 and 8.

Flatté, S. M., Bracher, C., and Wang, G.-Y. (**1994**). “Probability-density functions of irradiance for waves in atmospheric turbulence calculated by numerical simulation,” J. Opt. Soc. Am. A **11**, 2080–2092.

Frehlich, R., Cornman, L., and Sharman, R. (**2001**). “Simulation of three-dimensional turbulent velocity fields,” J. Appl. Meteorol. **40**, 246–258.

Gilbert, K. E., Raspet, R., and Di, X. (**1990**). “Calculation of turbulence effects in an upward-refracting atmosphere,” J. Acoust. Soc. Am. **87**, 2428–2437.

Gozani, J. (**1985**). “Numerical solution for the fourth-order coherence function of a plane wave propagating in a two-dimensional Kolmogorovian medium,” J. Opt. Soc. Am. A **2**, 2144–2151.

Hill, R. J., and Frehlich, R. G. (**1997**). “Probability distribution of irradiance in the onset of strong scintillation,” J. Opt. Soc. Am. A **14**, 1530–1540.

Hugon-Jeannin, Y. (**1992**). “Simulation numérique de la propagation d’ondes acoustiques en milieu turbulent (Numeric simulation of wave propagation in turbulent medium),” Ph.D. thesis, Ecole Centrale de Lyon, France.

Jakeman, E. (**1986**). *Wave Propagation and Scattering*, edited by B. J. Uscinski (Oxford University Press, Oxford, UK), pp. 1–381.

Jakeman, E., and Pusey, P. N. (**1976**). “A model for non-Rayleigh sea echo,” IEEE Trans. Antennas Propag. **24**, 806–814.

Jenu, M. Z. M., and Bebbington, D. H. O. (**1994**). “Fourth-moment calculation of optical propagation in a turbulent atmosphere with use of the split-step method,” J. Opt. Soc. Am. A **11**, 2862–2870.

Juvé, D., Blanc-Benon, P., and Chevret, P. (**1992**). “Numerical simulations of sound propagation through a turbulent atmosphere,” *5th Long Range Sound Propagation Symposium*, Milton Keyes, England. Available at http://ncpa.olemiss.edu/long-range-sound-propagation-lrsp/ (Last viewed March 26, 2012).

Knepp, D. L. (**1983**). “Multiple phase-screen calculation of the temporal behavior of stochastic waves,” Proc. IEEE **77**, 722–737.

Macaskill, C., and Ewart, T. E. (**1984**). “Computer simulation of a two-dimensional random wave propagation,” IMA J. Appl. Math. **33**, 1–15.

Martin, J., and Flatté, S. (**1988**). “Intensity images and statistics from numerical simulation of wave propagation in 3-D random media,” Appl. Opt. **27**, 2111–2126.

Martin, J., and Flatté, S. (**1990**). “Simulation of point-source scintillation through three-dimensional random media,” J. Opt. Soc. Am. A **7**, 838–847.

McLaren, J. R. W., Thomas, J. C., Mackintosh, J. L., Mudge, K. A., Grant, K. J., Clare, B. A., and Cowley, W.G. (**2012**). “Comparison of probability density functions for analyzing irradiance statistics due to atmospheric turbulence,” Appl. Opt. **51**, 5996–6002.

Norris, D., Wilson, D., and Thomson, D. (**2001**). “Atmospheric scattering for varying degrees of saturation and turbulent intermittency,” J. Acoust. Soc. Am. **109**, 1871–1880.

Ostashev, V. (**1997**). *Acoustics in Moving Inhomogeneous Media* (E & FN Spon, London), Chap. 6.

Ostashev, V. E., and Wilson, D. K. (**2000**). “Relative contributions from temperature and wind velocity fluctuations to the statistical moments of a sound field in a turbulent atmosphere,” Acta Acust. **86**, 260–268.

Ostashev, V., Wilson, D., Liu, L., Aldridge, D., Symons, N., and Marlin, D. (**2005**). “Equations for finite-difference, time-domain simulation of sound propagation in moving inhomogeneous media and numerical implementation,” J. Acoust. Soc. Am. **117**, 503–517.

Rivet, B., Girin, L., and Jutten, C. (**2007**). “Log-Rayleigh distributions: A simple and efficient statistical representation of log-spectral coefficients,” IEEE Trans. Audio, Speech, Lang. Process. **15**, 796–802.

Rytov, S. M., Kravtsov, Y. A., and Tatarski, V. I. (**1989**). *Principles of Statistical Radiophysics* (Springer, Berlin), Vol. 3–4.

Salomons, E. M., Blumrich, R., and Heimann, D. (**2002**). “Eulerian time-domain model for sound propagation over a finite-impedance ground surface: Comparison with frequency-domain models,” Acta. Acust. Acust. **88**, 483–492.

Spivack, M., and Uscinski, B. J. (**1988**). “Accurate numerical solution of the fourth-moment equation for very large values of Γ,” Ann. Math. Stat. **33**, 1187–1192.

Spivack, M., and Uscinski, B. J. (**1989**). “The split step solution in random wave propagation,” J. Comput. Appl. Math. **27**, 349–361.

Stacy, E. W. (**1962**). “A generalisation of the gamma distribution,” Ann. Math. Stat. **33**, 1187–1192.

Tatarski, V. I. (**1961**). *Wave Propagation in a Turbulent Medium* (McGraw-Hill, New York), Chap. 7.

Tatarski, V. I. (**1971**). “The effects of the turbulent atmosphere on wave propagation” (translated from Russian by the Israel Program for Scientific Translations, Jerusalem, 1971), Chap. 4. Available from the U.S. Department of Commerce, National Technical Information Service, Springfield, VA, 22151.

Tur, M. (**1982**). “Numerical solutions of the fourth moment of a plane wave propagating in a random medium,” J. Opt. Soc. Am. **72**, 1683–1691.

Van Renterghem, T. (**2003**). “The finite-difference time-domain method for simulation of sound propagation in a moving medium,” Ph.D. thesis, Universiteit Gent.

Van Renterghem, T., and Botteldooren, D. (**2003**). “Numerical simulation of the effect of trees on downwind noise barrier performances,” Acta. Acust. Acust. **89**, 764–778.

Wilson, D. (**1998**). “Turbulence models and the synthesis of random fields for acoustic wave propagation calculations,” ARL Technical Report No. ARL-TR-1677, pp. 1–60.

Wilson, D. K., and Liu, L. (**2004**). “Finite-difference, time-domain simulation of sound propagation in a dynamic atmosphere,” ERDC/CREEL Technical Report No. TR-04-12, pp. 1–64.

Yeh, K. C., Liu, C. H., and Youakim, M. Y. (**1975**). “A theoretical study of the ionospheric scintillation behavior caused by multiple scattering,” Radio Sci. **10**, 97–106, doi:10.1029/RS010i001p00097.